RSC Advances

This article can be cited before page numbers have been issued, to do this please use: Q. Zhang, K. Cheng, L. Wen, K. Guo and J. Chen, *RSC Adv.*, 2016, DOI: 10.1039/C6RA02512A.

ROYAL SOCIETY OF CHEMISTRY

www.rsc.org/advances

DOI: 10.1039/C6RA02512A

Study on the Precipitating and Aging Processes of $CuO/ZnO/Al_2O_3$ Catalysts Synthesized in Micro-impinging Stream Reactors

Qing-Cheng Zhang[a], Kun-Peng Cheng[a], Li-Xiong Wen[a,b,*],

Kai Guo[b], Jian-Feng Chen[a,b]

[a]*State Key Laboratory of Organic-Inorganic Composites, Beijing University of Chemical Technology, Beijing 100029, China.*

[b]*Research Center of the Ministry of Education for High Gravity Engineering and Technology, Beijing University of Chemical Technology, Beijing 100029, China.*

[*]Corresponding author. Tel.: +86-10-64443614; Fax: +86-10-64434784.

E-mail: wenlx@mail.buct.edu.cn

View Article Online
DOI: 10.1039/C6RA02512A

Abstract

$CuO/ZnO/Al_2O_3$ catalyst precursors were precipitated in a novel micro-impinging stream reactor (MISR) and a traditional stirred tank reactor (STR), respectively, followed by a period time of aging in the mother liquid. Being different from the simultaneous precipitating and aging of catalyst precursors within the same STR reactor, these two processes occurred in two separate containers in the MISR route, hence providing a more uniform and steady environment for both precipitating and aging processes on top of the higher micromixing efficiency and better process control of MISR. Therefore, substantial changes in the phase compositions and microstructures of the catalyst precursors were obtained with MISR, which resulted in smaller and more homogeneous catalyst particles with larger BET surface area and specific copper surface area, better Cu/Zn dispersion as well as higher catalytic activity when compared to those prepared in STR. The aging process also played an important role for the catalyst preparation and it could be controlled more easily and precisely in MISR route to form more desirable phase structure, morphology and eventually more superior catalytic performance in methanol synthesis for the final catalysts.

Keywords: Micro-impinging stream reactor; $CuO/ZnO/Al_2O_3$ catalysts; Precursors; Aging; Methanol synthesis

View Article Online
DOI: 10.1039/C6RA02512A

1. Introduction

Methanol is an important solvent and feedstock for the production of many chemicals such as formaldehyde, dimethyl ether, acetic acid, and a wide variety of other products.[1] It can also be used as a fuel additive and a clean burning fuel.[2] Industrial production of methanol from synthesis gas (a mixture of $CO/CO_2/H_2$) is mainly carried out over $CuO/ZnO/Al_2O_3$ catalysts at 200-300 ^oC and 5-10 MPa.[3,4] It is generally suggested that the particle size, specific surface area and Cu/Zn dispersion of $CuO/ZnO/Al_2O_3$ catalysts are the most important factors influencing the catalytic process.[5-7] Commercially, $CuO/ZnO/Al_2O_3$ catalysts are prepared by co-precipitation method in stirred tank reactors using aqueous solutions of metal nitrates and sodium carbonate to generate mixed Cu/Zn/Al hydrocarbonate precursors, followed by calcination and reduction processes to form the active $Cu/ZnO/Al_2O_3$ catalysts.[8] Constant pH condition is required in the catalyst synthesis to avoid independent or sequential precipitation of Cu^{2+} and Zn^{2+}, which prevents homogeneous distribution of both species in the precipitate.[9,10] Additionally, other conditions like temperature,[11,12] reactant concentration[13] and stirring speed[14] will also play significant roles on the physicochemical properties of the precursors and, in turn, the catalytic activity of the final catalysts. However, it is hard to precisely control this big set of parameters for one specific precipitation process in traditional stirred reactors. Even under the so-called "constant" precipitating conditions in drop-adding stirred reactors, the chemical potential of the reactants vary spatially and temporally when a droplet of the precipitating agent is added into the reactor, in which precipitates and dissolved ions

View Article Online
DOI: 10.1039/C6RA02512A

already coexist.[15] In addition, it was also found high levels of supersaturation, which are the thermodynamic driving force of phase transition, are necessary in the precipitation of crystal particles because of the highly nonlinear dependency of the nucleation rate on supersaturation.[16] During the conventional precipitation in stirred tank reactor (STR), local supersaturation is created when a droplet of precipitating agent is added into the other solution, and then vanishes through intensive stirring. A rapid micromixing is hence essential for the formation of uniform supersaturation level and consequently the product quality; however, it is difficult to achieve a rapid micromixing in traditional stirred reactors due to their poor mixing and mass transfer performance.[17] When the precipitating agent is added into the reactor quickly, a distinct feed rich zone will be formed near the feed pipe and result in an uneven concentration distribution, thus fast reactions may have already occurred or completed before the reactants accomplish homogeneous mixing.[18] On the other hand, a slow addition of fresh feed will lead to a wide residence time distribution and backmixing (the addition rates during the $CuO/ZnO/Al_2O_3$ catalyst synthesis are usually kept at 5-10 mL/min or even smaller).[12,13,19,20] As a consequence, the initial precipitates formed in stirred batch reactors may differ significantly, which can further lead to different microstructures and properties of $CuO/ZnO/Al_2O_3$ catalysts.

The precipitation of $CuO/ZnO/Al_2O_3$ catalyst precursors is often followed by an aging step. During the aging process, the precipitate remains in contact with its mother liquid and several reactions may take place at the same time, which can strongly affect the properties and consequently the catalytic performance of the final catalyst.[8,21,22]

View Article Online
DOI: 10.1039/C6RA02512A

Firstly, the initially formed precipitates will slowly transform by partial dissolution/re-precipitation reactions, and a recrystallization will occur at the same time accompanying with a change in color from blue to bluish green and, as expected, a change in chemical composition, particle size and morphology.[23,24] Secondly, a mixture of intermixed hydrocarbonates such as rosasite $(Cu,Zn)_2(OH)_2CO_3$ and aurichalcite $(Cu,Zn)_5(OH)_6(CO_3)_2$ will be formed through exchange reactions between the preformed phases.[10,25] Here, the efficient incorporation of Zn into malachite forming rosasite (zincian malachite) is regarded as the key to CuO/ZnO catalysts preparation, since a significant amount of atomically distributed Zn in rosasite will lead to an effective stabilization of the Cu phase and thus highly active CuO/ZnO catalysts will be obtained after thermal decomposition.[10,26] Therefore, the aging of fresh precipitates is also a crucial step for the synthesis of homogeneous $CuO/ZnO/Al_2O_3$ catalysts, and hence a uniform and steady environment will play a key role for the aging process as well as the quality of the final products. However, the aging environment in STR-operation mode is barely uniform or stable not only because of the simultaneous precipitating and aging processes but also the poor micromixing performance in STR. All precipitated particles get accumulated in STR for the whole precipitation process (it usually lasts ~20 min or even longer in the drop-adding method),[13,19,20,27] and the aging of precursors has already started before the precipitation is completed, which can lead to an inhomogeneous product distribution, as the initially formed precursors may differ significantly from the phase formed at the end of the precipitation.

A micro-impinging stream reactor (MISR) was built and applied to prepare

$CuO/ZnO/Al_2O_3$ catalysts for methanol synthesis in our previous studies.[28,29] The MISR is constructed with two steel capillaries connected to a commercial T-junction, but no tube is connected to the T-junction outlet, which provides a big-sized channel to lead the reacted precipitates into sample collectors for the next step. The two streams impinge on each other directly inside the T-junction to create a quick and constant supersaturation level and therefore a more homogeneous nucleation environment for the quick precipitating process, which may have been completed within the T-junction chamber. Therefore, the following aging process will have a uniform and steady environment. MISR also offers a better process control on reactant concentration, pH, volumetric flow rates and etc., and the residence time distribution for both of precipitating and aging processes is sharp, hence a better product quality of $CuO/ZnO/Al_2O_3$ catalysts will be achieved. In addition, unlike most of micro-structured devices such as microchannel reactor,[30] microfluidic reactor[31] and micromixer,[32] which are difficult to be fabricated due to their complicated configuration or easy to have severe blocking problems during the precipitation process due to the tiny channels inside the reactors, MISR can be easily constructed and has negligible blocking problem because of its bigger geometric dimensions and faster stream flows as compared to conventional microreactors.

In previous work, $CuO/ZnO/Al_2O_3$ catalysts have been prepared in MISR with better microstructures and properties as well as higher catalytic activity in methanol synthesis than those prepared in STR,[29] as a result of the intensified micromixing within the MISR reactor for the precipitating process as well as a more uniform and steady

View Article Online
DOI: 10.1039/C6RA02512A

environment for the subsequent aging process. In this work, we combined fast precipitation and freeze-drying to investigate the phase transitions during the first seconds of the precipitation, and then provided a detailed study on the effects of post-precipitation processes on the properties and activity of $CuO/ZnO/Al_2O_3$ catalysts and their precursors produced in MISR and traditional STR, respectively.

2. Experimental

2.1. Materials

Copper nitrate trihydrate $Cu(NO_3)_2{\cdot}3H_2O$ was purchased from Sinopharm Chemical Reagent Co. Ltd., China. Zinc nitrate hexahydrate $Zn(NO_3)_2{\cdot}6H_2O$, aluminum nitrate nonahydrate $Al(NO_3)_3{\cdot}9H_2O$ and sodium carbonate anhydrous Na_2CO_3 were provided by Beijing Reagent Factory, China. All reagents were of analytical grade and used without further purification.

2.2. Catalysts preparation

Ternary $CuO/ZnO/Al_2O_3$ catalyst precursors were prepared in MISR, which was the same as reported previously[29] by co-precipitation as follows: A solution of metal nitrates (C=0.8 mol/L, with a molar ratio of Cu/Zn/Al = 4.5/4.5/1) and aqueous sodium carbonate (C=1.15 mol/L) were injected into MISR simultaneously at a constant volumetric flow rate of 80 mL/min and impinged into each other by using two constant-flux pumps. The precipitation was conducted at room temperature and exactly controlled pH of 7.0 measured in the effluent of MISR. After impinging and precipitation within MISR, the precipitates were collected into a stirred and heated glass beaker filled with a small amount of deionized water. The suspension was then further

View Article Online
DOI: 10.1039/C6RA02512A

aged at 80 °C for a certain length of time (0, 10, 30, 60, 120 min) under vigorously stirring. After aging, the precursors were filtered and washed with deionized water for several times, and then dried overnight at 110 °C. Finally, the dried precursors were calcined at 350 °C for 4 h to obtain the $CuO/ZnO/Al_2O_3$ catalysts, which were then pelletized under a pressure of 10 MPa and crushed to 20-40 meshes for methanol synthesis.

The co-precipitation was also performed through a traditional route by simultaneously dropping two aqueous solutions containing metal nitrates and sodium carbonate, respectively, into a glass beaker filled with a small amount of deionized water under vigorous stirring at 80 °C. The metal nitrates solution was added at a rate of 5 mL/min, while the adding rate of the Na_2CO_3 solution was controlled to maintain the desired pH (7.0) in the mother liquid. After complete addition of the solutions, the suspension was further aged under continuous stirring at 80 °C for 0, 10, 30, 60 and 120 min, respectively. The post-processes were as same as those in the MISR route.

In addition, in order to investigate the phase transitions occurred during the first seconds of the precipitation, a part of non-aged precipitates were filtrated immediately after complete precipitation and no washing procedure was applied so that to minimize possible effects on the solids. The precipitates were then dried overnight in the freeze-dryer for subsequent analyses.

2.3. Characterization

Powder X-ray diffraction (XRD) analysis was carried out on a Bruker D8 Advance X-ray diffractometer using Cu-Kα radiation (λ≈1.54 Å) and scanning 2θ range from 10-

View Article Online
DOI: 10.1039/C6RA02512A

80 °.

Fourier transform infrared spectra (FT-IR) were measured in the range of 4000-400 cm^{-1} using the KBr disc technique on a PE2000 FT-IR spectrometer.

The particle morphologies were observed with a JEOL 3010 transmission electron microscopy (TEM) operated at 300 KV. The samples were ultrasonically dispersed in high purity ethanol and then deposited onto ultrathin carbon-coated nickel grids.

The temperature-programmed reduction (TPR) experiments were performed with an Autochem II 2920 multifunctional adsorption instrument. The samples (50 mg) were firstly purged with Ar for 0.5 h to remove physically absorbed water and then reduced in 10 vol.% H_2/Ar mixture gas (30 mL/min) at a heating rate of 10 ^oC /min up to 600 ^oC. The consumption of H_2 was analyzed by gas chromatograph (SP-2100A, China) equipped with a thermal conductivity detector (TCD).

X-ray photoelectron spectra (XPS) were conducted with an ESCALAB 250 spectrometer using Al-Kα radiation. The binding energies were calculated with respect to C 1s peak at 284.8 eV.

The specific surface area (S_{BET}) of the calcined catalysts was calculated by the BET method from nitrogen adsorption-desorption isotherms obtained with an ASAP 2010 surface area analyzer (Micromeritics Instrument Corporation, USA). All samples were pretreated under vacuum at 200 ^oC for 2 h.

The exposed copper surface area (S_{Cu}) was determined by N_2O reactive frontal chromatography (N_2O-RFC) and carried out with a Micromeritics AutoChem 2920 instrument through the method proposed by Gao et al.[33] The catalysts (0.1 g) were

first reduced with 10 vol.% H_2/Ar mixture (30 mL/min) at 350 ^oC for 2 h, followed by purging with Ar for 30 min and cooling to 65 ^oC. The reduced catalysts were then exposed to N_2O (30 mL/min) for 1 h to oxidize surface copper atoms to Cu_2O. After that the samples were flushed with Ar to remove the N_2O and cooled to room temperature. Finally, the Cu_2O at the surface was reduced back to metallic Cu at 350 ^oC in the H_2/Ar flow (30 mL/min). The S_{Cu} was calculated from the amount of consumed H_2 during the reduction steps, assuming a molar stoichiometry of N_2O/Cu_s = 2 and a value of 1.4×10^{19} Cu atoms/m^2 as the copper atoms density.[34]

2.4. Catalytic activity test

The catalytic performance of CO hydrogenation was carried out in a stainless steel tubular fixed-bed reactor (internal diameter = 1 cm), which was heated in a tube furnace controlled to ±0.1 ^oC by a programmable temperature controller. 1.0 g $CuO/ZnO/Al_2O_3$ catalyst diluted with 2.0 g inert quartz sand was placed in the constant temperature zone of the reactor. The sample was firstly reduced in situ with 10 vol.% H_2/N_2 at programmed temperature, which was raised from room temperature to 250 ^oC and then maintained at 250 ^oC for 6 h under atmospheric pressure. After reduction, the syngas of 33 vol.% CO and 67 vol.% H_2 was switched as feed gas with the space velocity of 4000 mL/(g_{cat} ħ) and the catalytic test was performed under 5.0 MPa and 250 ^oC to synthesize methanol. The outlet gas from the reactor was quantitatively analyzed every 30 min with a computer-interfaced online gas chromatograph (Shanghai Linghua Electronics Institute, GC-9890B), which was equipped with a Porapak T column (3 mm × 2 m) connected to a TCD detector using H_2 as carrier gas. The effluents from the reactor

View Article Online
DOI: 10.1039/C6RA02512A

were kept at 200 ºC before entering GC to avoid product condensation. The catalytic activity was evaluated at the steady state of reacting system.

The conversion of CO is defined as:

$$\frac{(mol\ carbon\ monoxide\ converted\ to\ all\ products)}{(mol\ carbon\ monoxide\ in\ the\ feed\ gas)} \quad (1)$$

The selectivity to methanol is defined as:

$$\frac{(mol\ produced\ methanol)}{(mol\ carbon\ monoxide\ converted\ to\ all\ products)} \quad (2)$$

3. Results and discussion

Since the precipitating and aging processes are separated in the MISR route for the preparation of $CuO/ZnO/Al_2O_3$ catalysts, it can provide a uniform and steady environment for both processes and, therefore, offers the possibility to investigate the phase transitions of the initial precipitates right after the precipitation by a freeze-drying technology, as well as the aging behaviors for different length of time and their effects on the structures and properties of the precursors and final catalysts, which is not possible with the traditional stirred tank reactor (STR) route due to the simultaneous precipitating and aging processes.

3.1 Phase structure analysis of the initial precipitates prepared in different routes

The XRD patterns of fresh precipitates, which were quenched immediately in freeze-dryer, are shown in Fig. 1. In addition to the intensive diffraction peaks of the byproduct $NaNO_3$, which existed because no washing procedure was applied, crystalline sodium zinc carbonate $Na_2Zn_3(CO_3)_4$ (JCPDS No. 86-0607) was identified

View Article Online
DOI: 10.1039/C6RA02512A

as the kinetically metastable product in MISR. The typical peak for Cu precursor was not observed because the solid formation started with the initial precipitation of amorphous copper-containing species.[21,35] However, the initial precipitate formed in STR was mostly X-ray amorphous, except for the diffraction peak at $2\theta = 34.0$ °ascribed to hydrozincite $Zn_5(OH)_6(CO_3)_2$ (JCPDS No. 72-1100) or aurichalcite (JCPDS No. 82-1253) along with $NaNO_3$ diffraction peaks. Such phase structure differences of the initial precipitates prepared in these two different routes was mainly due to the different micromixing performances and co-precipitation modes in MISR and STR, respectively. Previous studies indicated that $Na_2Zn_3(CO_3)_4$ was quite unstable in the mother liquid and would easily transform into the more thermodynamically stable zinc-enriched hydrocarbonates (hydrozincite or aurichalcite).[36-39] In the STR-operation mode, all precipitated particles remained in the same reaction vessel for the whole precipitation process, a chemical phase transition of $Na_2Zn_3(CO_3)_4$ induced by water or thermal treatment would have already taken place for a long residence time before the precipitation was completed (the co-precipitation process in this study took ~15 min), and this phase transition would be accelerated by vigorous stirring.[38] Therefore, the initial precipitates formed at different precipitating time and the different places of STR might differ significantly in chemical compositions and phase structures. By contrast, the whole precipitation in MISR was very fast (the residence time was ~ 1 s and the whole process took only ~1 min), and the characteristic micromixing time of MISR was in the range of 1~10 ms,[28] thus more homogeneous precipitates would be obtained in MISR.

View Article Online
DOI: 10.1039/C6RA02512A

3.2 Characterization of precursors aged for different length of time

Residual sodium in precursors is known to poison the catalysts and to enhance the sintering of metallic particles in methanol synthesis, thus the washing treatment is of crucial importance for the preparation of highly active $CuO/ZnO/Al_2O_3$ catalysts.[40] For this reason, the precursors in the subsequent sections were analyzed after repeated washing treatment with deionized water and then dried in oven overnight.

Fig. 2a shows the XRD patterns of precursors prepared in MISR and aged for different length of time. It was found that, after washing and oven-drying processes, the diffraction peaks belonging to $Na_2Zn_3(CO_3)_4$ were mostly disappeared and the complete removal of crystalline $NaNO_3$ was achieved as the diffraction peak at $2\theta = 29.0°$ was not observed anymore, which was very strong for the samples without washing as shown in Fig. 1. Therefore, a structural rearrangement of the system took place when the fresh precipitate was exposed to water and it was unlikely that any $Na_2Zn_3(CO_3)_4$ would have remained in the sample after being vigorously stirred and washed in STR-route, followed by drying at 110 ^oC overnight.[36-39] When the precipitates were intensively stirred in the mother liquid for a certain aging time (10, 30, 60 or 120 min), $Na_2Zn_3(CO_3)_4$ was completely converted into zinc-enriched hydrocarbonate phases. Meanwhile, the crystallization of malachite $Cu_2(OH)_2CO_3$ and rosasite from amorphous copper-containing species would start as well, accompanying with a color change from blue to bluish green. It was found that the characteristic peaks of malachite (JCPDS No. 41-1390) and rosasite (JCPDS No. 18-1095) at $2\theta = 14.8°$, 17.6°, 24.2° and 31.9° appeared after 30 min aging and increased in intensities with time, which is in good

View Article Online
DOI: 10.1039/C6RA02512A

accordance with the studies of Farahani et al.[13] who proposed that further increase in aging time after the appearance of color change would cause a progressive crystalline growth as a result of Ostwald ripening. In addition, the Zn-Al hydrotalcite $Zn_6Al_2(OH)_{16}CO_3 \cdot 4H_2O$ (JCPDS No. 38-0486) represented by the diffraction peaks at $2\theta = 11.5°$ and $23.3°$ was observed for precursors aged for 120 min. Therefore, aging of the freshly precipitated solids would eventually result in a mixture of hydrocarbonate phases, which could strongly affect the microstructures and consequently the catalytic performance of the final catalyst.

The XRD patterns of precursors prepared in STR aged for different length of time are shown in Fig. 2b. No noticeable variation was found in the XRD patterns of the hydrocarbonate phases through the washing treatment except for the removal of crystalline $NaNO_3$, and then STR samples followed the same transitional tracks in aging process as those prepared in MISR. In addition, a slight shift of the malachite diffraction peak near $2\theta = 32°$ ($20\bar{1}$ peak) to higher angles was observed when the aging time was increased from 30 min to 60 min (Fig. 2c), which was correlated with the substitution chemistry of malachite as Zn^{2+} is incorporated into malachite structure forming rosasite.[10,41] Therefore, the exchange reactions between the preformed phases took place during the aging of precursors, which would enhance the Cu/Zn dispersion of final catalysts. However, the $20\bar{1}$ peak shifted back to lower angles when the precursor was aged for 120 min, which was due to the formation of Zn-Al hydrotalcite as shown in the XRD patterns.

Compared to the MISR-route, all precursors prepared in STR exhibited much

View Article Online
DOI: 10.1039/C6RA02512A

sharper copper-enriched hydrocarbonates (malachite and rosasite) diffraction peaks indicating larger crystallites according to Scherrer equation. In addition, a considerable shift of $20\bar{1}$ peak towards higher angles ($2\theta = 32.1°$) was observed for the precursor prepared in MISR as compared to STR samples, which suggested a highest degree of Cu-substitution by Zn in rosasite phase should be achieved in MISR-route after 60 min aging of precursor, and thus $CuO/ZnO/Al_2O_3$ catalyst of fine dispersion was obtained. Such differences in the compositions and microstructures of precursors were traced back to the different pathways of solid formation for two precipitation routes. As discussed earlier, in the drop-adding stirred reactor, particle growth takes place when a droplet of precipitating agent is added into the reactor in which precipitates have already existed.[42] On the other hand, the intense impinging in MISR creates a fast and uniform micromixing as well as a high supersaturation level, which favors nucleation rather than crystal growth, thus results in smaller and more uniform particles in the precipitation.[43,44] In addition, the aging mechanism has shown that no binary precipitates can be directly obtained,[9] however, MISR can be used to form a pseudo-homogeneous precipitate with the best possible distribution of Cu- and Zn-intermediates due to its homogeneous nucleation environment, which will further accelerate the exchange reactions between the preformed phases and, in turn, favor the Cu/Zn dispersion of final catalysts.

A comparison of the FT-IR spectra for precursors prepared at different conditions (different routes and aging times) is shown in Fig. 3. All samples displayed a weak absorption band around 1630 cm^{-1} ascribed to the bending vibration of water. For the

MISR-prepared samples (Fig. 3a), there was a small peak at 1385 cm^{-1} representing the asymmetric N-O vibration in the non-aged precursor, which was due to the existence of a small amount of gerhardtite $Cu_2(OH)_3NO_3$ generated by the reaction between $Cu(OH)_2$ and NO_3^-. However, an unambiguous discrimination of poorly crystallized samples on the basis of XRD patterns is difficult due to their high similarity in crystal structures, thus gerhardtite was not detected in XRD analysis in Fig. 2. Gerhardtite was believed to exert adverse effect for production of active catalyst by forming larger copper particles (i.e. sintering effect).[11] Fortunately, gerhardtite would then slowly react upon aging with hydroxide and carbonate to form amorphous georgeite $Cu(OH)_2CO_3$ (the chemical formula of georgeite was the same as that of malachite),[21] thus the asymmetric N-O vibration disappeared when the precipitate was aged for 10 min. The strong absorption bands of the amorphous precursors (0, 10 min aging) around 1480 and 837 cm^{-1} were quite similar to those of georgeite reported by Shen et al.[20,27] In addition, the characteristic bands in the region of 1520-1390 cm^{-1} were attributed to asymmetric C-O stretching vibration, whereas the bands around 835 cm^{-1} were ascribed to out-of-plane OCO bending mode.[41] Increasing the aging time from 10 min to 30 min forced the asymmetric C-O stretching vibration around 1480 cm^{-1} shift to 1499 cm^{-1}, which was mainly ascribed to the recrystallization of amorphous georgeite, either directly crystallized to malachite or transformed into rosasite.[20,27,35] All crystallized samples displayed the spectra with only small differences in position and intensity, hence the characterization of a phase mixture would be complicated for the carbonate bands originating from the malachite, rosasite and aurichalcite that overlapped

View Article Online
DOI: 10.1039/C6RA02512A

significantly. However, previous studies[45,46] have suggested that the incorporation of Zn^{2+} into the malachite lattice forming rosasite would result in a shift of the asymmetric C-O stretching vibration (around 1500 cm^{-1}) to higher wavenumber. Compared to other precursors, the precursor aged for 60 min showed the higher wavenumber (1506 cm^{-1}) of the asymmetric C-O stretching vibration; therefore, a more homogeneous microstructure of the $CuO/ZnO/Al_2O_3$ catalyst might be obtained in the MISR with 60-min aging of precursor.

For the samples prepared in STR (Fig. 3b), it was found that the non-aged precursor displayed a very small peak at 1385 cm^{-1} representing the asymmetric N-O vibration; however, its intensity was much lower than the MISR-prepared sample (Fig. 3a), which was due to the gradual transformation of gerhardtite to georgeite during the precipitation process in STR as already discussed. Therefore, it confirmed that several reactions took place in the long residence time before the complete precipitation in STR. The small differences of IR spectra in positions and intensities (Fig. 3a and 3b) indicated that the two precipitation routes generated precipitates and precursors with different chemical compositions and phase structures, which was mainly due to the different micromixing performances, nucleation environments and residence time distributions of the STR and MISR, respectively.

3.3 Characterization of calcined catalysts after aging for different length of time

The XRD patterns of the calcined catalysts prepared at different conditions are shown in Fig. 4. It showed that the phase structures of the catalyst samples were mainly composed of CuO (JCPDS No. 48-1548) and ZnO (JCPDS No. 36-1451). The overlap

View Article Online
DOI: 10.1039/C6RA02512A

of diffraction peaks for CuO at 2θ = 35.4° and ZnO at 2θ = 36.2° indicated the formation of CuO-ZnO solid solution. Besides, the typical peaks for Al_2O_3 (2θ = 19°, 45°) were not observed, suggesting that Al_2O_3 might exist in an amorphous state.[5] For the MISR-prepared catalysts (Fig. 4a), it was found that the non-aged catalyst exhibited sharp diffraction peaks indicating large crystallite sizes, which was mainly due to the existence of $Na_2Zn_3(CO_3)_4$ and gerhardtite in the precursor as already discussed in the XRD analysis (Fig. 2a) and IR spectra (Fig. 3a) on the precursors.[11] However, only weak peaks ascribed to ZnO could be found in the catalyst obtained from the 10-min aged precursor and the absence of CuO diffraction peaks in XRD pattern indicated that CuO was poorly crystallized. When the aging time was prolonged, the diffraction peaks ascribed to CuO increased in intensities, which were correlated to the remarkable crystalline growth of copper-enriched hydrocarbonate phases in the corresponding precursors (Fig. 2a). On the other hand, a very weak CuO diffraction peak at 2θ = 38.8 ° was observed for the non-aged catalyst prepared in STR (Fig. 4b), which was due to the gradual transformation of $Na_2Zn_3(CO_3)_4$ and gerhardtite during the precipitation process into zinc-enriched hydrocarbonates and amorphous georgeite, respectively. However, it should be concerned that these important phase transitions would also take place when the precipitate was vigorously stirred after complete precipitation in MISR (~1 min). The separated precipitating and aging processes in the MISR-route provided a uniform and steady environment for both processes and, therefore, a better product quality of CuO/ZnO/Al_2O_3 catalysts might be achieved. In addition, for the catalysts aged for the same length of time (10, 30, 60, 120 min) after the complete precipitation,

View Article Online
DOI: 10.1039/C6RA02512A

sharper diffraction peaks were observed for the catalysts prepared in STR as compared to MISR-route, which suggested larger CuO and ZnO crystallites were obtained in STR. Therefore, both precipitating and aging of precursors played important roles in determining the phase structures of the precursors and final catalysts.

TPR profiles were given in Fig. 5 to investigate the reduction patterns of copper species for the $CuO/ZnO/Al_2O_3$ catalysts prepared at different conditions. Samples prepared in both routes exhibited a broad peak without any shoulders in the range of 200-300 ^oC, which was obtained from the reduction of CuO. Under the experimental conditions in this work, ZnO and Al_2O_3 would not be reduced.[47] For the MISR-prepared catalysts (Fig. 5a), the non-aged catalyst showed a reduction peak at 265 ^oC, and a shift of reduction temperature towards 238 ^oC was observed when the aging time was increased to 10 min, which was correlated to smaller CuO crystallites in the prepared catalyst as demonstrated by the weak CuO diffraction peaks in XRD patterns (Fig. 4a). In addition to the particle size effect, the shift of reduction peak to lower temperature might also be caused by the better copper dispersion of the mixed oxides.[48,49] Therefore, the shift of reduction peak to lower temperature might be mainly owing to the higher zinc content into the malachite structure forming rosasite when aging time was prolonged (from 10 min to 60 min) as already discussed in XRD patterns (Fig. 2a) and IR analysis (Fig. 3a), thus favoring the copper dispersion and finally improving the reducibility of $CuO/ZnO/Al_2O_3$ catalysts. In addition, compared with the narrow reduction peaks for the $CuO/ZnO/Al_2O_3$ catalysts obtained from MISR route, the TPR profiles of the catalysts prepared in STR (Fig. 5b) were broader and shifted to higher

View Article Online
DOI: 10.1039/C6RA02512A

reduction temperature, suggesting much larger CuO particles with a much wider size distribution were obtained in STR. Previous studies concerning the reducibility of copper-based catalysts for methanol synthesis and methanol steam reforming have revealed that a high catalytic activity is associated with good reducibility of catalysts;[50,51] therefore, higher catalytic performance would be expected for the MISR-prepared catalysts.

Fig. 6 illustrates the typical XPS spectra of Cu $2p_{3/2}$ levels of the $CuO/ZnO/Al_2O_3$ catalysts prepared at different conditions. The binding energy (BE) range for the main Cu $2p_{3/2}$ peak was around 933.5 eV, generally with characteristic satellite peaks between 940 and 945 eV due to the electron shake-up process.[52] Various studies[53-55] have shown that the positions of these peaks depend on the chemical composition and crystalline structure of the catalyst, and particularly on the near environment of Cu^{2+}. The binding energy of Cu $2p_{3/2}$ for pure CuO was 934.0 eV, which was higher than those of ternary $CuO/ZnO/Al_2O_3$ catalysts, indicating that CuO and other metal oxides were not simply physically mixed in the $CuO/ZnO/Al_2O_3$ catalysts but an interaction between them was present. This is because that the electronegativity of Cu (1.90) is stronger than that of Zn (1.65), which induced the migration of electron cloud to Cu and finally resulted in a shift of Cu $2p_{3/2}$ to lower BE.[53] In addition, it was found that the MISR-prepared catalyst that was aged for 60 min displayed lower BE compared to other catalysts, which was mainly attributed to the enhanced interaction between CuO and ZnO because of their fine particle size and better Cu/Zn dispersion.

TEM images of the $CuO/ZnO/Al_2O_3$ catalysts prepared at different conditions and

View Article Online
DOI: 10.1039/C6RA02512A

after methanol synthesis are shown in Fig. 7. The samples showed very similar morphology and comprised agglomerates of round and oval particles. TEM analysis of MISR-prepared catalysts as a function of aging time revealed a decrease of primary particle size from ~10 nm (non-aged) to ~6 nm (10 min aging) (Fig. 7a,b), which was well consistent with the XRD analysis in Fig. 4a. It was also found that, after aging for 60 min, the catalyst produced in MISR contained mostly round particles with a mean size of 8-10 nm (Fig. 7c), whereas slightly larger and more irregular particles were obtained in STR route (Fig. 7d). This observation agreed well with the XRD analysis (Fig. 4) and TPR results (Fig. 5), which indicated that larger and ununiformed catalyst particles were obtained in STR due to its poor mixing and mass transfer performance.[17] In addition, the TEM images showed that significant aggregation of catalyst particles took place after methanol synthesis reaction for both MISR- and STR-prepared catalysts (Fig. 7e, 7f), but with a more severe aggregation for the STR-prepared catalyst. Such aggregation might be caused by the highly exothermic effect of the methanol synthesis reaction and would result in less active sites and a decrease of catalytic activity during the synthesis process.[56-58]

3.4 Catalytic activities of the calcined catalysts after aging for different length of time

The physicochemical properties of the $CuO/ZnO/Al_2O_3$ catalysts prepared at different conditions are summarized in Table 1. It was found that the non-aged catalyst prepared in MISR displayed the lowest S_{BET} (54.1 m^2/g) and S_{BET} increased remarkably when the catalysts were aged for a period of time. The maximum S_{BET} of 141.6 m^2/g

View Article Online
DOI: 10.1039/C6RA02512A

was obtained when the aging t = 10 min, and a reduction of S_{BET} was observed with further increasing aging time due to the slight increase in particle size as already described in XRD analysis (Fig. 4a) and TEM images (Fig. 7). The exposed copper surface area (S_{Cu}) is a more important parameter for Cu-based catalysts since metallic copper is generally regarded as the main active component. Table 1 showed that the non-aged catalyst had the lowest S_{Cu} of 7.5 m^2/g. However, S_{Cu} for the MISR-prepared catalysts did not follow the same trend as that of $S_{BET.}$ The maximum S_{Cu} of 22.4 m^2/g was observed for the MISR-prepared catalyst aged for 60 min, which can provide more catalytically active sites due to its better Cu/Zn dispersion. Further increase in aging time to 120 min caused the remarkable growth of crystallite size and decreased the catalyst S_{Cu}. In addition, the sample prepared in STR, which has poor micromixing and mass transfer performance, displayed much lower S_{BET} and S_{Cu} than MISR-prepared catalyst (both aged for 60 min) due to its larger particle size and poor Cu/Zn dispersion as already discussed in previous sections.

The catalytic performances in methanol synthesis via CO hydrogenation for the $CuO/ZnO/Al_2O_3$ catalysts prepared at different conditions are also shown in Table 1. It demonstrated that the catalytic activity (CO conversion, X_{CO}) would be enhanced greatly with increasing S_{Cu} for the MISR-prepared samples, which was mostly enhanced with increasing aging time until it reached a proper length of time (60 min). But the positive influence of S_{Cu} on the CH_3OH selectivity (S_{MeOH}) was much slighter. Therefore, the non-aged MISR-prepared catalyst had the lowest X_{CO} and S_{MeOH}, while the highest X_{CO} and S_{MeOH} were achieved by the MISR-prepared catalyst with 60 min

View Article Online
DOI: 10.1039/C6RA02512A

aging-treatment. Such results agreed well with the previous observations that the aging process with proper time would lead to more homogeneous microstructure of the precursors and final $CuO/ZnO/Al_2O_3$ catalyst, and the well dispersed CuO could enhance the synergy reaction with ZnO crystallites and hence improve the catalytic activity of the catalyst. Table 1 also showed that the MISR-prepared catalyst with 60 min aging-treatment had significantly higher S_{BET}, S_{Cu} and X_{CO} than those of the STR-prepared catalyst with 60 min aging-treatment, which agreed well with its larger particle size and poorer Cu/Zn dispersion for the STR products and clearly demonstrated the advantages of the MISR-route over the STR-route for catalyst preparation.

It is widely accepted that the methanol synthesis via CO hydrogenation is a structure-sensitive catalytic reaction. The different catalytic performances of these catalysts were associated with the combining effects of their different phase structures, crystallite sizes, Cu/Zn dispersion, exposed copper surface area and specific surface area as already discussed in previous sections. In addition, defects on the surface and/or in the bulk structure, such as microstrain, impurities, and structural disorder were also suggested to be responsible for the catalytic performances of the copper-based catalysts, which needs further investigation.[59-62] Therefore, both precipitating and aging processes will play key roles for the catalytic performance of the final $CuO/ZnO/Al_2O_3$ catalysts.

4. Conclusions

This study examined the specific effects of washing and aging treatments on the

View Article Online
DOI: 10.1039/C6RA02512A

structures and properties of the precipitated precursors and the final $CuO/ZnO/Al_2O_3$ catalysts with two different co-precipitation routes: via micro-impinging stream reactor (MISR) or traditional stirred tank reactor (STR). The MISR route conducted the precipitating and aging processes in two separated steps, thus providing a uniform and steady environment for both of them. In addition, significantly intensified micromixing performance could be achieved with MISR. Therefore, catalysts with smaller crystallite size, better Cu/Zn dispersion, higher BET surface area and specific Cu surface area, and superior catalytic activity in methanol synthesis were obtained with MISR as compared to the STR route. It was also found that the washing and aging treatments affected the microstructure and consequently the catalytic performance of $CuO/ZnO/Al_2O_3$ catalysts remarkably. A mixture of sodium zinc carbonate and amorphous copper-containing species were formed in the initial stage of precipitation. Aging of fresh precipitates induced a structural rearrangement of sodium zinc carbonate to the more thermodynamically stable hydrozincite or aurichalcite, while amorphous copper-containing species were gradually transformed into crystal malachite and rosasite accompanied with a color change from blue to bluish green. In addition, increasing the aging time of precursors (from 0 to 60 min) resulted in more uniform microstructures of the $CuO/ZnO/Al_2O_3$ catalysts, which exhibited higher specific Cu surface area and more superior catalytic performance in methanol synthesis. However, further increase in aging time (120 min) of precursor caused remarkable growth of crystallite size and lowered the catalytic activity of the final catalysts.

View Article Online
DOI: 10.1039/C6RA02512A

Acknowledgments

The authors gratefully acknowledge the financial support provided by National Natural Science Foundation of China (Nos. 21376015, 21576012 and 91334206).

References

1 E. E. Ortelli, J. Wambach and A. Wokaun, *Appl. Catal., A*, 2001, **216**, 227-241.
2 G. A. Olah, *Angew. Chem., Int. Ed.*, 2005, **44**, 2636-2639.
3 Y. L. Zhang, Q. Sun, J. F. Deng, D. Wu and S. Y. Chen, *Appl. Catal., A*, 1997, **158**, 105-120.
4 P. Mierczynski, T. P. Maniecki, K. Chalupka, W. Maniukiewicz and W. K. Jozwiak, *Catal. Today*, 2011, **176**, 21-27.
5 P. Gao, F. Li, F. K. Xiao, N. Zhao, W. Wei, L. S. Zhong and Y. H. Sun, *Catal. Today*, 2012, **194**, 9-15.
6 G. J. Millar, I. H. Holm, P. J. R. Uwins and J. Drennan, *J. Chem. Soc., Fataday Trans.*, 1998, **94**, 593-600.
7 M. Kurtz, N. Bauer, C. Büscher, H. Wilmer, O. Hinrichsen, R. Becker, S. Rabe, K. Merz, M. Driess, R. Fischer and M. Muhler, *Catal. Lett.*, 2004, **92**, 49-52.
8 M. Behrens and R. Schlögl, *Z. Anorg. Allg. Chem.*, 2013, **639**, 2683-2695.
9 M. Behrens, D. Brennecke, F. Girgsdies, S. Kißner, A. Trunschke, N. Nasrudin, S. Zakaria, N. F. Idris, S. B. A. Hamid, B. Kniep, R. Fischer, W. Busser, M. Muhler and R. Schlögl, *Appl. Catal., A*, 2011, **392**, 93-102.
10 S. Zander, B. Seidlhofer and M. Behrens, *Dalton Trans.*, 2012, **41**, 13413-13422.
11 J. L. Li and T. Inui, *Appl.Catal., A*, 1996, **137**, 105-117.
12 C. Baltes, S. Vukojević and F. Schüth, *J. Catal.*, 2008, **258**, 334-344.
13 B. V. Farahani, F. H. Rajabi, M. Bahmani, M. Ghelichkhani and S. Sahebdelfar, *Appl. Catal., A*, 2014, **482**, 237-244.
14 G. Simson, E. Prasetyo, S. Reiner and O. Hinrichsen, *Appl.Catal., A*, 2013, **450**, 1-12.
15 X. H. Liu, Y. Y. Bao, Z. P. Li and Z. M. Gao, *Chin. J. Chem. Eng.*, 2010, **18**, 588-599.
16 H.-C. Schwarzer and W. Peukert, *AIChE J.*, 2004, **50**, 3234-3247.
17 J. Bałdyga, J. R. Bourne and S. J. Hearn, *Chem. Eng. Sci.*, 1997, **52**, 457-466.
18 S. Bhattacharya and S. M. Kresta, *Chem. Eng. Res. Des.*, 2004, **82**, 1153-1160.
19 G. C. Shen, S. I. Fujita and N. Takezawa, *J. Catal.*, 1992, **138**, 754-758.
20 G. C. Shen, S. I. Fujita, S. Matsumoto and N. Takezawa, *J. Mol. Catal. A: Chem.*, 1997, **124**, 123-136.
21 B. Bems, M. Schur, A. Dassenoy, H. Junkes, D. Herein and R. Schlögl, *Chem. - Eur. J.*, 2003, **9**, 2039-2052.
22 E. N. Muhamad, R. Irmawati, Y. H. Taufiq-Yap, A. H. Abdullah, B. L. Kniep, F. Girgsdies and T. Ressler, *Catal. Today*, 2008, **131**, 118-124.
23 S. Klokishner, M. Behrens, O. Reu, G. Tzolova-Müller, F. Girgsdies, A. Trunschke and R. Schlögl, *J. Phys. Chem. A*, 2011, **115**, 9954-9968.

24 D. M. Whittle, A. A. Mirzaei, J. S. J. Hargreaves, R. W. Joyner, C. J. Kiely, S. H. Taylor and G. J. Hutchings, *Phys. Chem. Chem. Phys.*, 2002, **4**, 5915-5920.

25 B. L. Kniep, F. Girgsdies and T. Ressler, *J. Catal.*, 2005, **236**, 34-44.

26 M. Behrens, *J. Catal.*, 2009, **267**, 24-29.

27 S. I. Fujita, A. Satriyo, G. Shen and N. Takezawa, *Catal. Lett.*, 1995, **34**, 85-92.

28 Z. W. Liu, L. Guo, T. H. Huang, L. X. Wen and J. F. Chen, *Chem. Eng. Sci.*, 2014, **119**, 124-133.

29 Q. C. Zhang, Z. W. Liu, X. H. Zhu, L. X. Wen, Q. F. Zhu, K. Guo and J. F. Chen, *Ind. Eng. Chem. Res.*, 2015, **54**, 8874-8882.

30 N. Kockmann, J. Kastner and P. Woias, *Chem. Eng. J.*, 2008, **135, Supplement 1**, S110-S116.

31 H. Wang, X. Li, M. Uehara, Y. Yamaguchi, H. Nakamura, M. Miyazaki, H. Shimizu and H. Maeda, *Chem. Comm.*, 2004, 48-49.

32 M. Schur, B. Bems, A. Dassenoy, I. Kassatkine, J. Urban, H. Wilmes, O. Hinrichsen, M. Muhler and R. Schlögl, *Angew. Chem., Int. Ed.*, 2003, **42**, 3815-3817.

33 P. Gao, F. Li, N. Zhao, F. K. Xiao, W. Wei, L. S. Zhong and Y. H. Sun, *Appl. Catal., A*, 2013, **468**, 442-452.

34 Z. L. Yuan, L. N. Wang, J. H. Wang, S. X. Xia, P. Chen, Z. Y. Hou and X. M. Zheng, *Appl. Catal., B*, 2011, **101**, 431-440.

35 A. M. Pollard, M. S. Spencer, R. G. Thomas, P. A. Williams, J. Holt and J. R. Jennings, *Appl. Catal., A*, 1992, **85**, 1-11.

36 S. Kaluza, M. Behrens, N. Schiefenhövel, B. Kniep, R. Fischer, R. Schlögl and M. Muhler, *ChemCatChem*, 2011, **3**, 189-199.

37 S. Kaluza, M. K. Schröter, R. Naumann d'Alnoncourt, T. Reinecke and M. Muhler, *Adv. Funct. Mater.*, 2008, **18**, 3670-3677.

38 S. Kaluza and M. Muhler, *Catal. Lett.*, 2009, **129**, 287-292.

39 S. Kaluza and M. Muhler, *J. Mater. Chem.*, 2009, **19**, 3914-3922.

40 K. W. Jun, W. J. Shen, K. S. Rama Rao and K. W. Lee, *Appl. Catal., A*, 1998, **174**, 231-238.

41 M. Behrens, F. Girgsdies, A. Trunschke and R. Schlögl, *Eur. J. Inorg. Chem.*, 2009, **2009**, 1347-1357.

42 L. Wantha and A. E. Flood, *J. Cryst. Growth*, 2011, **318**, 117-121.

43 J. Nvlt, *Cryst. Res. Technol.*, 1995, **30**, 737-745.

44 D. V. Alexandrov, *Chem. Eng. Sci.*, 2014, **117**, 156-160.

45 D. Stoilova, V. Koleva and V. Vassileva, *Spectrochimica Acta Part A: Molecular and Biomolecular Spectroscopy*, 2002, **58**, 2051-2059.

46 Z. Li, S. W. Yan and H. Fan, *Fuel*, 2013, **106**, 178-186.

47 S. Velu, K. Suzuki, M. Okazaki, M. P. Kapoor, T. Osaki and F. Ohashi, *J. Catal.*, 2000, **194**, 373-384.

48 P. Gao, F. Li, F. K. Xiao, N. Zhao, N. N. Sun, W. Wei, L. S. Zhong and Y. H. Sun, *Catal. Sci. Technol.*, 2012, **2**, 1447-1454.

49 F. Meshkini, M. Taghizadeh and M. Bahmani, *Fuel*, 2010, **89**, 170-175.

50 X. M. Guo, D. S. Mao, G. Z. Lu, S. Wang and G. S. Wu, *Catal. Commun.*, 2011, **12**, 1095-1098.

51 P. Kurr, I. Kasatkin, F. Girgsdies, A. Trunschke, R. Schlögl and T. Ressler, *Appl. Catal., A*, 2008, **348**, 153-164.

52 J. W. Bae, S.-H. Kang, Y.-J. Lee and K.-W. Jun, *J. Ind. Eng. Chem.*, 2009, **15**, 566-572.

53 R. T. Figueiredo, A. Martínez-Arias, M. L. Granados and J. L. G. Fierro, *J. Catal.*, 1998, **178**,

View Article Online
DOI: 10.1039/C6RA02512A

146-152.

54 L. H. Zhang, C. Zheng, F. Li, D. G. Evans and X. Duan, *J. Mater. Sci.*, 2008, **43**, 237-243.

55 F. Garbassi and G. Petrini, *J. Catal.*, 1984, **90**, 106-112.

56 J. T. Sun, I. S. Metcalfe and M. Sahibzada, *Ind. Eng. Chem. Res.*, 1999, **38**, 3868-3872.

57 G. Prieto, J. D. Meeldijk, K. P. de Jong and P. E. de Jongh, *J. Catal.*, 2013, **303**, 31-40.

58 X. Zhai, J. Shamoto, H. Xie, Y. Tan, Y. Han and N. Tsubaki, *Fuel*, 2008, **87**, 430-434.

59 T. Ressler, B. L. Kniep, I. Kasatkin and R. Schlögl, *Angew. Chem., Int. Ed.*, 2005, **44**, 4704-4707.

60 I. Kasatkin, P. Kurr, B. Kniep, A. Trunschke and R. Schlögl, *Angew. Chem., Int. Ed.*, 2007, **46**, 7324-7327.

61 S. Natesakhawat, J. W. Lekse, J. P. Baltrus, P. R. Ohodnicki, B. H. Howard, X. Deng and C. Matranga, *ACS Catal.*, 2012, **2**, 1667-1676.

62 M. Behrens, S. Zander, P. Kurr, N. Jacobsen, J. Senker, G. Koch, T. Ressler, R. W. Fischer and R. Schlögl, *J. Am. Chem. Soc.*, 2013, **135**, 6061-6068.

View Article Online
DOI: 10.1039/C6RA02512A

Table 1. Physicochemical properties and catalytic activity of the catalysts prepared at different conditions.

Reactor	Aging time (min)	S_{BET} (m^2/g)	S_{Cu} (m^2/g)	X_{CO} (mol %)	S_{MeOH} (C-mol %)	Y_{MeoH} (mol %)
MISR	0	54.1	7.5	12.8	97.7	12.4
MISR	10	141.6	16.9	25.9	97.9	25.3
MISR	30	103.3	18.5	30.6	98.9	30.2
MISR	60	103.4	22.4	33.7	99.3	33.5
MISR	120	77.0	16.1	28.4	98.6	28.0
STR	60	64.7	13.4	27.2	98.8	26.8

Reaction conditions: T = 250 °C, V(CO):V(H_2) = 33:67, P = 5 MPa, GHSV = 4000 mL/(g_{cat}·h).

View Article Online
DOI: 10.1039/C6RA02512A

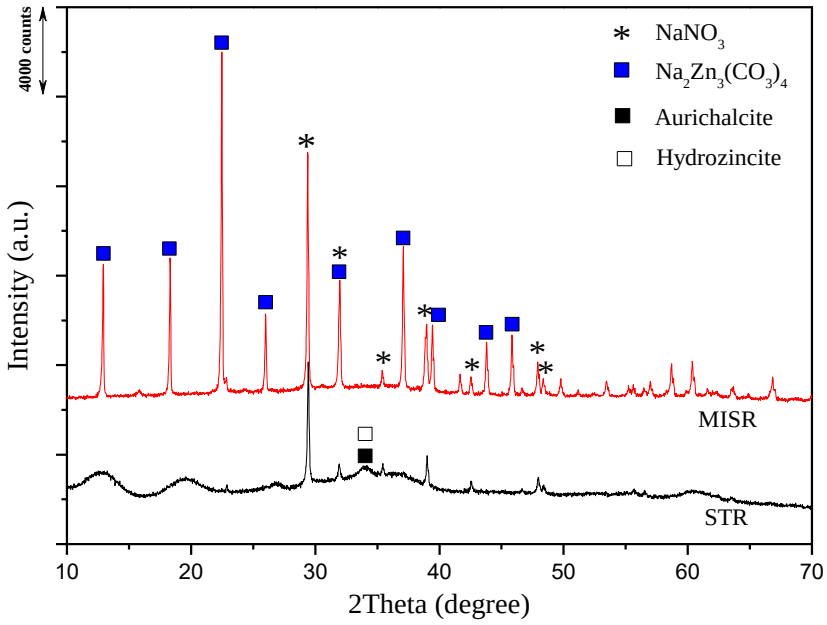

Fig. 1. XRD patterns of the initial precipitates formed in different reactors.

View Article Online
DOI: 10.1039/C6RA02512A

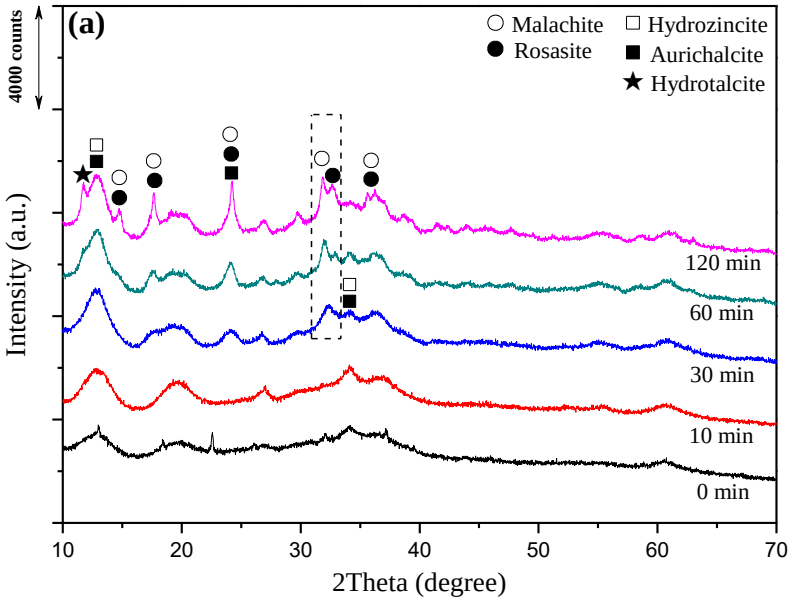

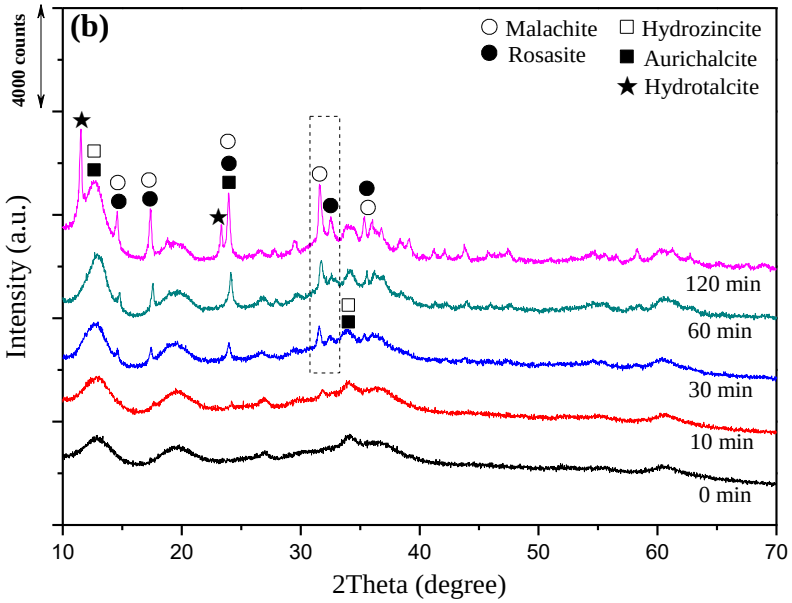

View Article Online
DOI: 10.1039/C6RA02512A

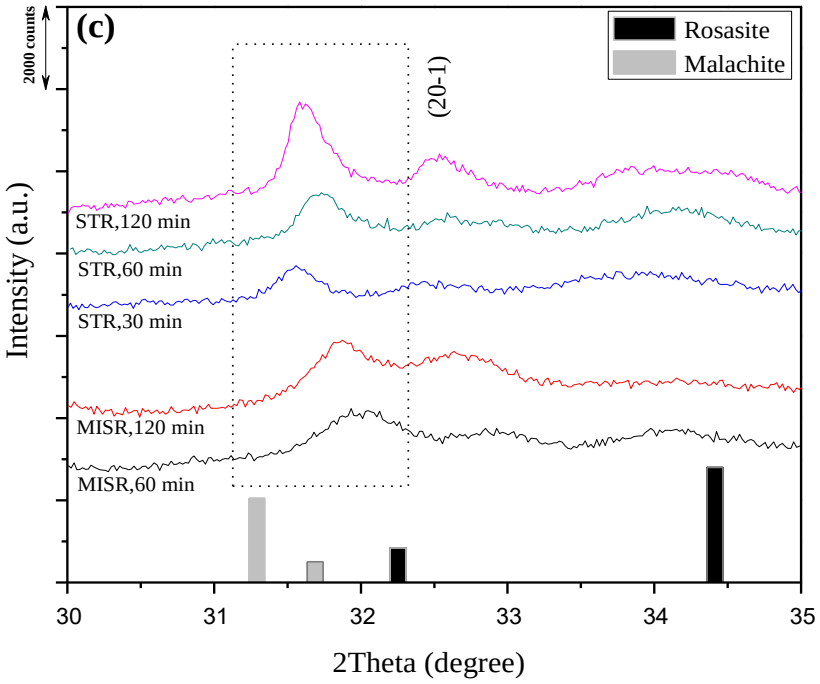

Fig. 2. XRD patterns of the catalyst precursors aged for different length of time: (a), MISR-prepared; (b), STR-prepared; (c), the position of $20\bar{1}$ peak.

View Article Online
DOI: 10.1039/C6RA02512A

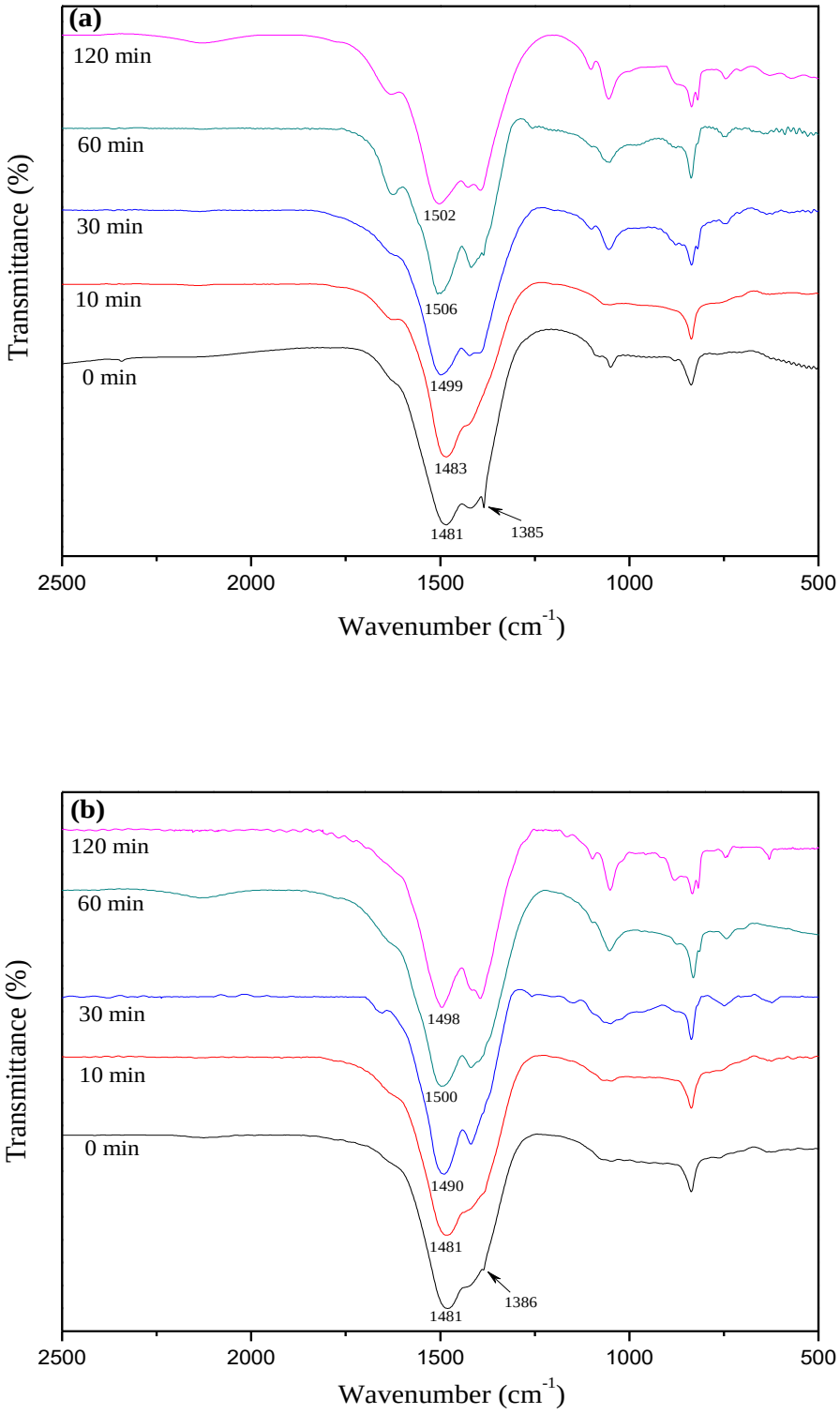

Fig. 3. IR spectra of the catalyst precursors aged for different length of time: (a), MISR-prepared; (b), STR-prepared.

View Article Online
DOI: 10.1039/C6RA02512A

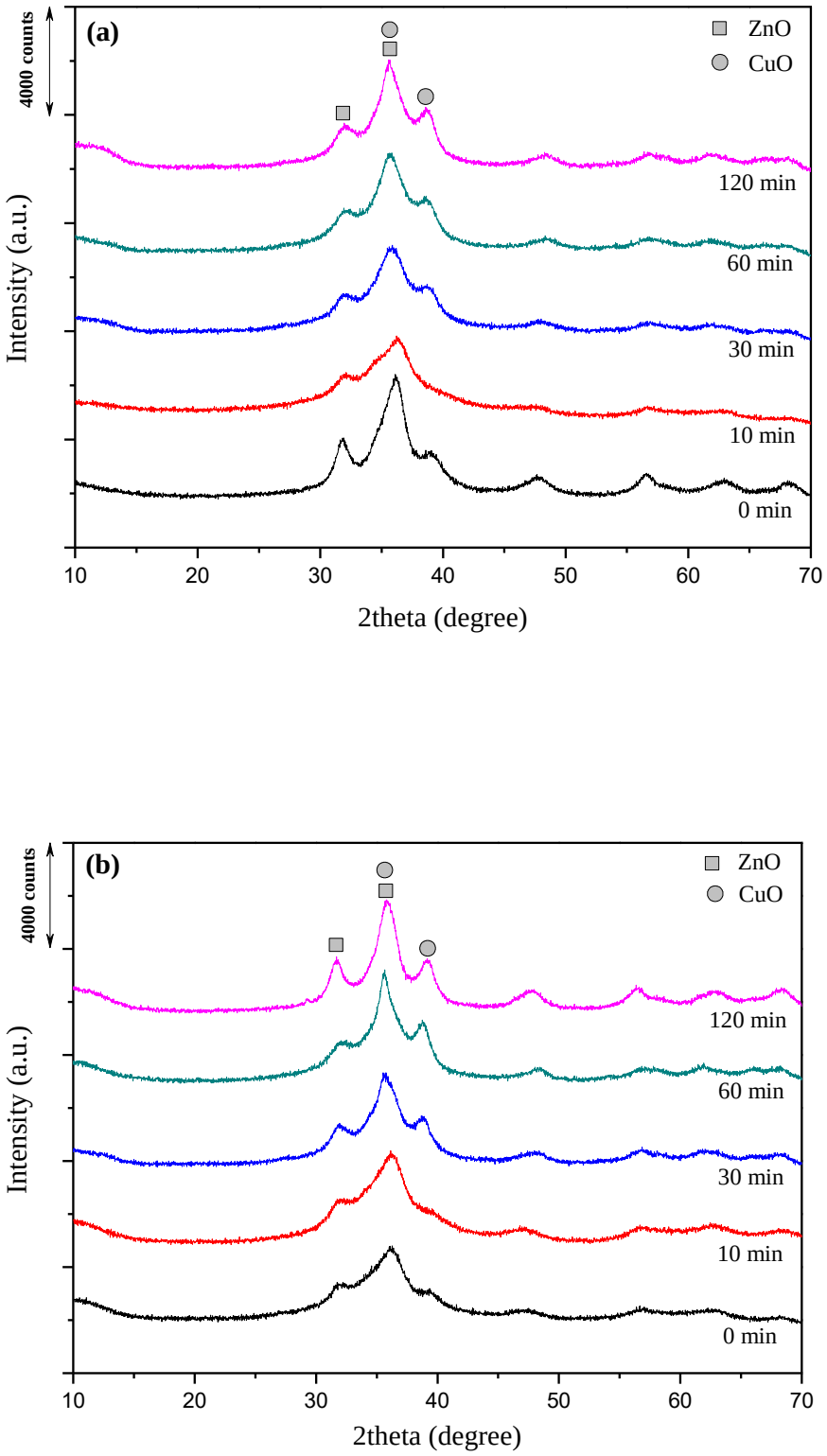

Fig. 4. XRD patterns of the CuO/ZnO/Al_2O_3 catalysts aged for different length of time: (a), MISR-prepared; (b), STR-prepared.

View Article Online
DOI: 10.1039/C6RA02512A

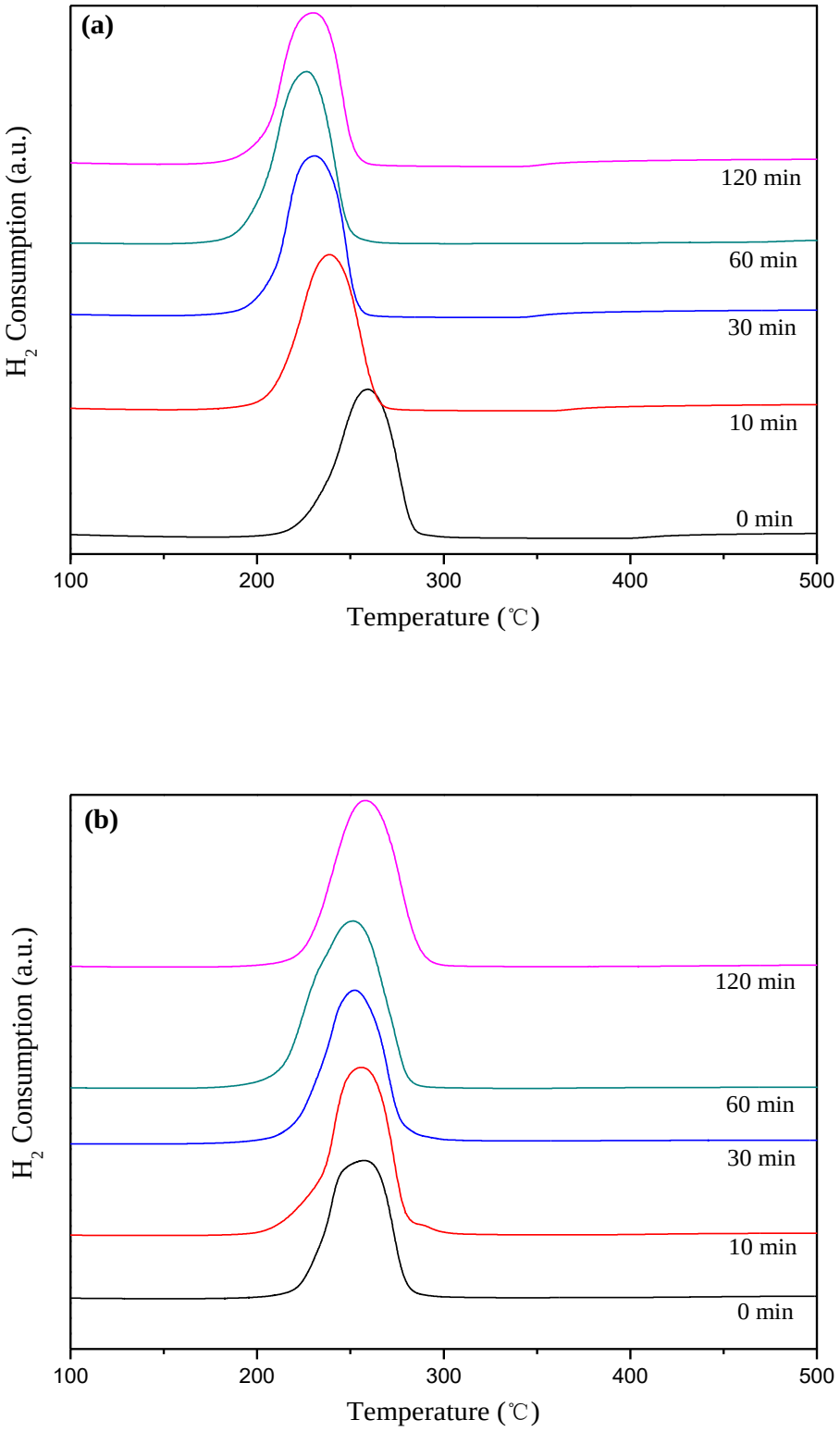

Fig. 5. TPR profiles of the $CuO/ZnO/Al_2O_3$ catalysts aged for different length of time:

(a), MISR-prepared; (b), STR-prepared.

View Article Online
DOI: 10.1039/C6RA02512A

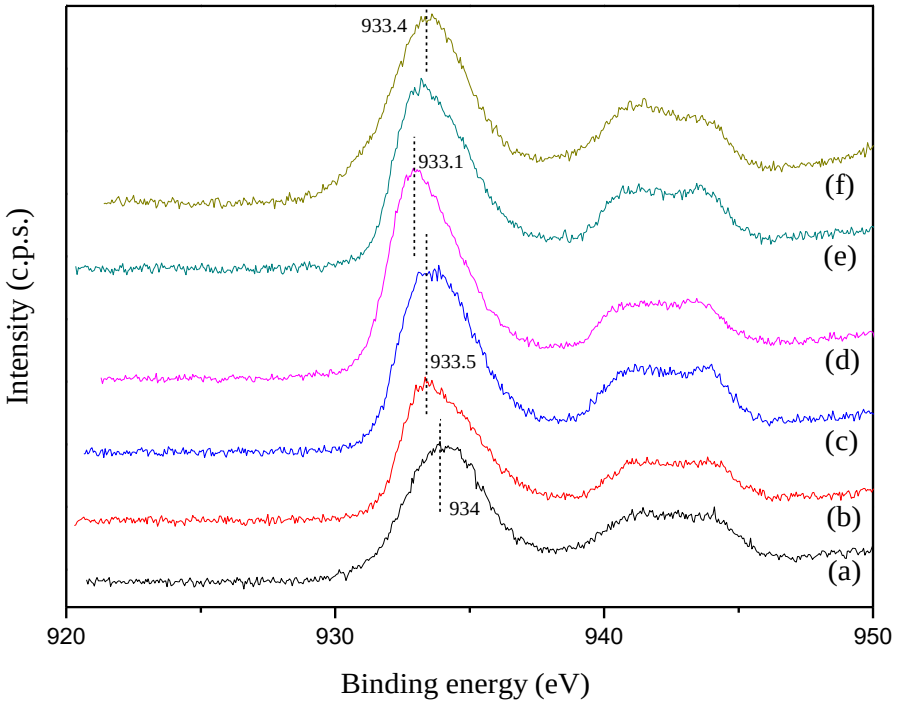

Fig. 6. XPS spectra of the $CuO/ZnO/Al_2O_3$ catalysts aged for different length of time: (a)-(e), MISR-prepared, aging t=0, 10, 30, 60, 120 min, respectively; (f), STR-prepared, aging t=60 min.

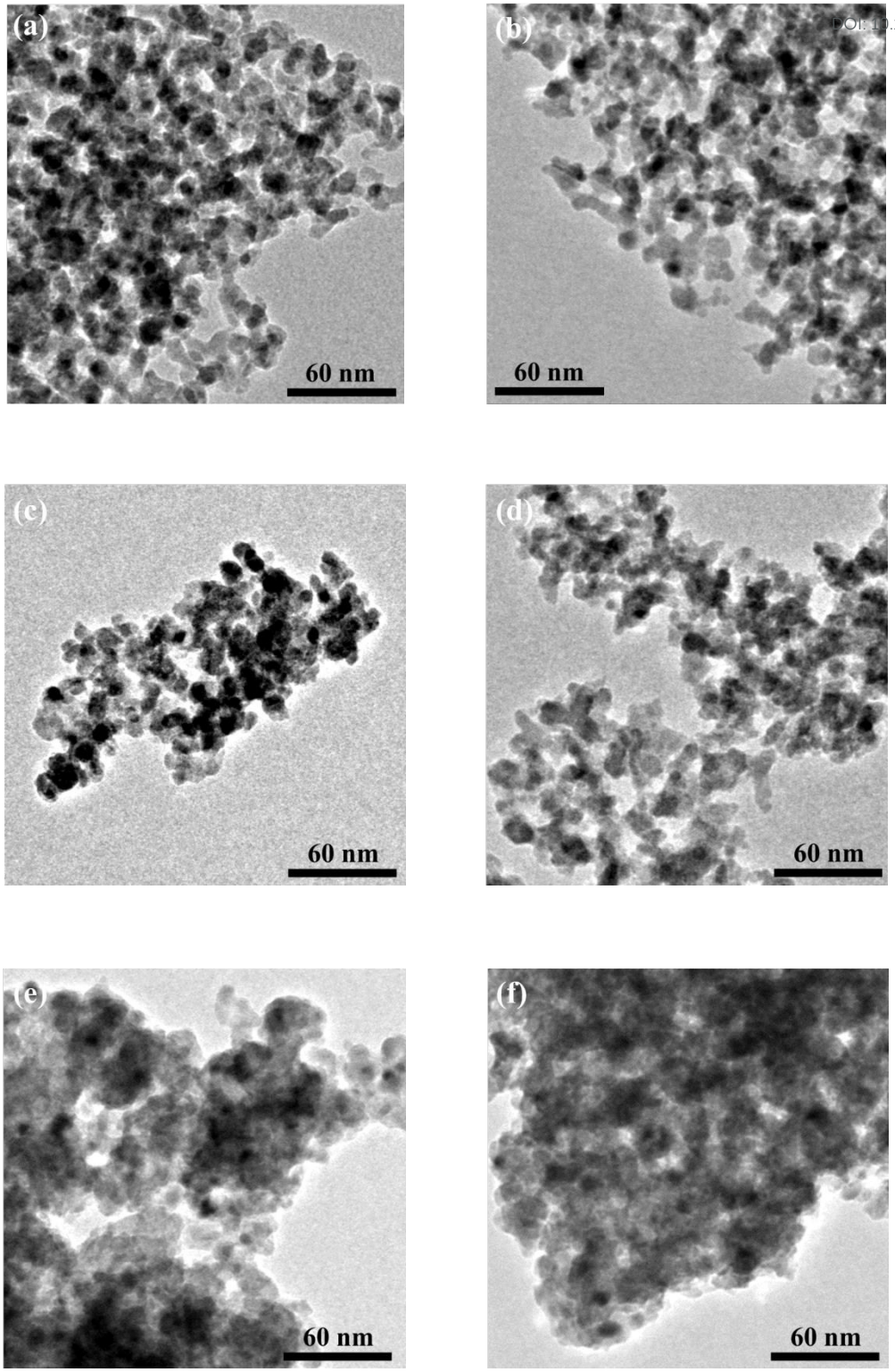

Figure 7. TEM images of different Cu-based catalysts: (a)-(c), MISR-prepared, aging t = 0, 10, 60 min, respectively, unreacted; (d), STR-prepared, t = 60 min, unreacted; (e), MISR-prepared, t = 60 min, reacted catalyst; (f), STR-prepared, t = 60 min, reacted catalyst.

View Article Online
DOI: 10.1039/C6RA02512A

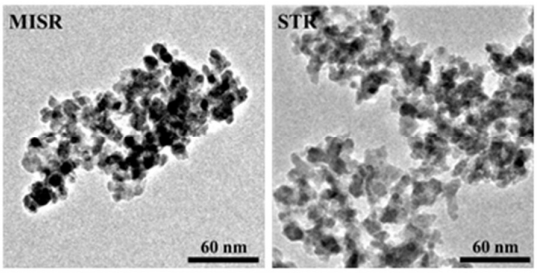

Precipitating and aging processes of $CuO/ZnO/Al_2O_3$ catalysts were performed more uniformly in micro-impinging stream reactors than in stirred reactors.